PLASMA FREQUENCY RADIATION IN TOKAMAKS

K. Swartz
I. H. Hutchinson
Kim Molvig

PFC/JA-79-10

PLASMA FREQUENCY RADIATION IN TOKAMAKS

K. Swartz
Department of Physics
Harvard University
Cambridge, Massachusetts 02138
and
Plasma Fusion Center
Massachusetts Institute of Technology
Cambridge, Massachusetts 02139

I. H. Hutchinson
Plasma Fusion Center and Francis Bitter
National Magnet Laboratory
Massachusetts Institute of Technology
Cambridge, Massachusetts 02139

Kim Molvig
Plasma Fusion Center and Nuclear
Engineering Department
Massachusetts Institute of Technology
Cambridge, Massachusetts 02139

Radiation from relativistic runaway electrons is considered as a source for plasma frequency radiation in tokamaks. Two specific emission mechanisms, Cerenkov emission, and radiation produced by nonlinear coupling of plasma and acoustic waves, are studied. In many cases the Cerenkov emission provides a reasonable spectral fit. It can also be used to measure the runaway current, and to estimate the runaway cutoff velocity. The nonlinear emission is found to be negligible unless the acoustic waves are enhanced by about two orders of magnitude above the thermal level (or the plasma waves correspondingly enhanced above their superthermal level). Some observations, though, indicate the need for significant nonlinear (or other) emission in addition to the Cerenkov emission. For some typical Alcator data, the Cerenkov model gives a runaway current of 2.5 percent of the ohmic current, and a cutoff energy of 1.5 MeV.

I. INTRODUCTION

In many Tokamaks radiation has been observed extending in frequency from the plasma frequency at the center of the discharge, to the electron cyclotron frequency at the outer edge of the plasma [1-5]. The characteristics of this radiation as it is presently observed are briefly summarized as follows. It occurs for $(\Omega_o/\omega_{po}) \geq 3/2$, where Ω and ω_p are the cyclotron and plasma frequencies, and subscript o denotes values at the plasma center. Its shape varies with $(\Omega/\omega_p)_o$, from a rather narrow (experimentally unresolved) feature near ω_{po} [2,5] for small $(\Omega/\omega_p)_o$, to much broader[1,2,5], sometimes double peaked[4]; structures at larger $(\Omega/\omega_p)_o$. Its intensity is typically several times the blackbody level for the corresponding electron temperature, and the extraordinary polarization intensity has been observed[4,5] to exceed the ordinary mode.

Several theories [6-10] have been proposed to explain this emission. The purpose of this paper is to examine and develop the two seemingly most cogent theories with enough realistic detail to make a direct comparison with experiment.

The first mechanism considered was proposed by Freund, Lee and Wu [6], and invokes the direct Cerenkov emission by relativistic runaways of extraordinary mode electromagnetic radiation; it is emitted over a broad range of frequencies. The second mechanism, proposed by Hutchinson, Molvig and Yuen [9], considers the nonlinear conversion of an elevated electrostatic plasma spectrum to electromagnetic emission, by scattering from thermal level ion-acoustic fluctuations; this process emits only just above the

plasma frequency at the source point.

In section II. the relevant equations governing the Cerenkov emission are given, and are related to an observed specific radiation intensity. It is shown that in many cases the intensity of radiation is approximately proportional to the total runaway current, and an approximate formula is presented.

Section III. develops and expands the nonlinear model, including a closely related decay process. This treatment is conditioned by knowledge of the Cerenkov emission, and it is shown that for the relationship between the runaway distribution and the plasma wave energy density predicted by the self-consistent theory of Molvig, Tekula and Bers[11], the nonlinear emission from scattering from thermal ion-acoustic fluctuations is small compared to the Cerenkov emission. Nonlinear conversion should be important only if a more elevated level of acoustic or plasma wave spectra exists.

In section IV. an attempt is made to reproduce the experimental spectra in shape and intensity from the Cerenkov emission. In some cases a reasonable fit can be found but only for rather specific parameters, thus providing tentative information on the cutoff energy of the runaway tail and the total current it carries.

In other cases, while partial agreement can be obtained, discrepancies in shape remain which appear to be unavoidable for the Cerenkov process. Section V. discusses these and other limitations.

II. CERENKOV EMISSION

A. Character of the Emission

The Cerenkov emission can be computed as the incoherent sum of emissions from the individual runaway electrons, moving along the magnetic field, in a cold, uniform plasma. The perpendicular velocity can be ignored because most of the emission comes from electrons for which $\gamma r_L/\lambda \ll 1$, where γ is the relativistic factor, r_L is the Larmor radius, and λ is the wavelength. The cold dielectric response is used because the radiation phase velocity is much greater than the electron thermal velocity. (Since the emission frequency $\omega < \Omega_E$, where Ω_E is the cyclotron frequency at the plasma edge, it is always well below the local upper hybrid resonance). The plasma is considered uniform, since the wavelength is small compared to field, density, and temperature scale lengths. The plasma is also optically thin to the Cerenkov emission; the small positive slope of the runaway distribution (see later) is so small that the amplification length for the extraordinary mode is much larger than a typical Tokamak minor radius.

The dispersion relation and the coherence condition are two constraints on the Cerenkov emission which account for many of its properties. The index of refraction, n, as a function of ω and $\cos\theta \equiv (\underset{\sim}{k}\cdot\underset{\sim}{B}/kB)$ (where $\underset{\sim}{k}$ is the wave vector, and $\underset{\sim}{B}$ is the magnetic field) is the Appleton-Hartree relation:

$$n^2(\omega^2,\cos^2\theta) =$$

$$1 - \left\{ \frac{2\left(\frac{\omega_p}{\omega}\right)^2 \left[1 - \left(\frac{\omega_p}{\omega}\right)^2\right]}{2\left[1 - \left(\frac{\omega_p}{\omega}\right)^2\right] - \left(\frac{\Omega}{\omega}\right)^2 \sin^2\theta \mp \left[\left(\frac{\Omega}{\omega}\right)^4 \sin^4\theta + 4\left(\frac{\Omega}{\omega}\right)^2 \cos^2\theta \left(1 - \left(\frac{\omega_p}{\omega}\right)^2\right)^2\right]^{1/2}} \right\} \quad (1)$$

where ω_p and Ω have their local values, and the minus sign defines the extraordinary (x) mode, the plus sign the ordinary (o) mode.

The coherence condition is (v is the velocity of the emitting particle):

$$\frac{\omega}{k} = v\cos\theta . \tag{2}$$

Equation (1) implies that for $\omega > \omega_p$, the frequencies observed, $n^2 > 1$ for the x mode, while $n^2 < 1$ for the o mode. Thus, only the extraordinary mode is emitted for $\omega > \omega_p$. Combining Eqs. (1) and (2), $v/c \equiv u(\omega, \cos\theta) = [n(\omega, \cos\theta)\cos\theta]^{-1}$. From Eq. (1), it follows that

$$\frac{\partial[n^2(\omega^2,\cos^2\theta)\cos^2\theta]}{\partial(\cos^2\theta)} > 0$$

for $\omega_p < \omega < \Omega$, so that u decreases as $\cos\theta$ increases, and a particle cannot radiate at frequency ω unless its velocity is greater than $u_{min}(\omega) = u(\omega, \cos\theta = 1)$. This quantity u_{min} is typically much greater than the electron thermal velocity, so that only the nonthermal tail radiates. As ω goes to ω_p, n goes to 1, and u_{min} becomes highly relativistic, the lowest frequency of emission corresponding to the highest possible $u = u_c$, the velocity at which the runaways are cut off.

Equations (1) and (2) can also be combined to find:

$$\cos^2\theta \pm \left(\frac{\omega}{\omega_p}, \frac{\omega}{\Omega}, u\right) = \left\{ 2\left[1-\left(\frac{\omega_p}{\omega}\right)^2\right]^2 u^2 - \left(\frac{\Omega}{\omega}\right)^2\left[2u^2 + (1-u^2)\left(\frac{\omega_p}{\omega}\right)^2\right] \pm \left(\frac{\omega_p}{\omega}\right)^2\left(\frac{\Omega}{\omega}\right)\left[4\left(1-\left(\frac{\omega_p}{\omega}\right)^2\right)u^2 + \left(\frac{\Omega}{\omega}\right)^2(1-u^2)^2\right]^{1/2}\right\} \Bigg/ 2u^2\left\{\left[1-\left(\frac{\omega_p}{\omega}\right)^2\right]^3 u^2 - \left(\frac{\Omega}{\omega}\right)^2\left[u^2 + (1-u^2)\left(\frac{\omega_p}{\omega}\right)^2\right]\right\} . \tag{3}$$

To get Eq. (3) the radical in Eq. (1) must be squared, so that the corresponding sign, referring to the choice of mode, is lost. While the sign

in Eq. (3) refers to one of two roots to a quadratic quation, it does not necessarily, as in (1), refer to one mode. Depending on its arguments, $\cos^2\theta_{\pm}$ may be acceptably double valued, single valued, or violate the requirement $0 \leq \cos^2\theta_{\pm} \leq 1$. However, when a single choice of sign satisfies this requirement for $\omega_p < \omega < \Omega$ (as is usually the case; see Fig. 1) it is identified with the x mode. A more convenient quantity for numerical computation is $n_{\pm}^2 \equiv [u^2\cos^2\theta_{\pm}]^{-1}$, which must satisfy:

$$n_{\pm}^2 u^2 \geq 1. \tag{4}$$

The quantity $\cos^2\theta_{\pm}$ can be studied numerically, and for typical parameters decreases as u increases for fixed ω, and as ω increases for fixed u:

$$(\cos^2\theta)_{min} = \cos^2\theta\ (\omega_{max},\ u = 1). \tag{5}$$

Many of the emission characteristics obtained from Eqs. (1) and (2) are summarized by the contour plot of $u(\cos\theta, \omega)$, shown in figure 1.

B. Spectral Emission and Isotropized Flux

The spectral source of radiation per unit volume S^x (erg./sec.-cm.^{3}-Hz.) is just the spectral power from each electron, $d\varepsilon/dt\ (u,\omega)$ (erg./sec.-Hz.), incoherently summed over the electron tail distribution function $f_T(u)$:

$$S^x(\omega) = \int f_T(u)\ \frac{d\varepsilon}{dt}\ (u,\omega)\ du\ . \tag{6}$$

The spectral power, $d\varepsilon/dt$, was first computed by Kolomenskii[12]; it is just $-q(\underset{\sim}{v} \cdot \underset{\sim}{E})_{\underset{\sim}{r} = \underset{\sim}{v}t}$, where q and $\underset{\sim}{r}$ are the particle charge and position, and the electric field $\underset{\sim}{E}$ includes dielectric shielding effects:

$$E_p(\underset{\sim}{k},\omega) = \frac{q}{2\pi^2\omega^2 i}\ T_{pq}^{-1}\ v_q\ \delta\left(\frac{\underset{\sim}{k} \cdot \underset{\sim}{v}}{\omega} - 1\right),$$

where

$$T_{pq} = \left(\frac{c^2}{\omega^2}\right)\left[k_p k_q - k^2 \delta_{pq}\right] + \varepsilon_{pq} ,$$

and $\underline{\underline{\varepsilon}}$ is the dielectric tensor.

The cold dielectric tensor is used, in which the tail electrons, whose density is negligible, are neglected. Inverting the Fourier transform, and taking the perpendicular velocity equal to zero, gives:

$$\frac{d\varepsilon}{dt} = \mathrm{Re}\, \frac{iq^2u^2}{\pi c} \int \omega d\omega \int \sin\theta \, d\theta \int n^2 dn \, \delta(n\, u \cos\theta - 1) \times$$

$$\left\{ \frac{n^4\cos^2\theta - n^2\varepsilon_1 \left[1 + \cos^2\theta\right] + \varepsilon_1^2 - \varepsilon_2^2}{\left[\varepsilon_1 \sin^2\theta + \varepsilon_3 \cos^2\theta\right]\left[n^2 - n_x^2(\omega,\cos\theta)\right]\left[n^2 - n_o^2(\omega,\cos\theta)\right]} \right\}, \qquad (7)$$

where

$$\varepsilon_1 \equiv 1 + \frac{\omega_p^2}{\Omega^2 - \omega^2} , \quad \varepsilon_2 \equiv \frac{\omega_p^2 \Omega}{\omega(\Omega^2 - \omega^2)} , \text{ and } \varepsilon_3 \equiv 1 - \frac{\omega_p^2}{\omega^2} .$$

In the angular integration, the delta function picks out the contributions from $\cos^2\theta_{\pm}$. These are the radiation terms which, when the real part of the integral over n is taken, are integrals over ω, whose integrands are:

$$\frac{d\varepsilon}{dt_{\pm}}(u,\omega) = \frac{q^2}{2c} u\omega \left\{ \left(1 - \frac{1}{\varepsilon_1 u^2}\right)^{\pm} \right.$$

$$\left. \frac{\left[\varepsilon_1\varepsilon_2 \left(\frac{\Omega}{\omega}\right) u^4 - \left(2\varepsilon_1\varepsilon_2 \left(\frac{\Omega}{\omega}\right) + \varepsilon_2^2\right) u^2 + \varepsilon_2 \left(\frac{\Omega}{\omega}\right)\right]}{u^2\varepsilon_1 \left[\left(\frac{\Omega}{\omega}\right)^2 \varepsilon_2^2 u^4 - 2\varepsilon_1 \left(\varepsilon_1^2 - \varepsilon_2^2 + \varepsilon_3^2\right) u^2 + 2\varepsilon_3 \left(2\varepsilon_1^2 + \varepsilon_2^2\right) u^2 + \varepsilon_2^2 \left(\frac{\Omega}{\omega}\right)^2\right]^{1/2}} \right\}, \qquad (8)$$

where the $\pm$ here correspond to the $\pm$ in (3).

From the radiation volume source S^x, the radiative flux F^x (erg./sec. - cm^2 - Hz.) corresponding to the observed quantity, must be found. To do this, the transport of the radiation must be considered. The maximum phase velocity angle at the source can be found from (5), and is typically about forty degrees. While there is a substantial difference between this angle and the local group velocity angle, the angle of interest is the group velocity angle at the edge, where the phase and group velocities are equal. Since the index of refraction decreases to one at the edge, the net effect is for the ray to bend away from the normal, towards the field, and the maximum ray angle that could be seen is less than forty degrees. Tokamak observations, though, are typically made within a small angular range about the direction perpendicular to the magnetic field ($\lesssim 2°$ in Alcator). Cerenkov emission must thus be reflected to be detected. The observed ratio of x to o polarized radiation is, in fact, consistent with a model where the ordinary emission is produced by polarization scrambling occuring during multiple reflections.[4] Because of the reflections, only the angle-integrated, or isotropic emission, rather than emission as a function of angle, is of interest.

The argument for isotropization is only important, of course, if the radiation can get out of the plasma. Total internal reflection can be a serious constraint on the emission.[13] In a slab model, none of the Cerenkov emission can get out; along the ray, $k_{\|}c/\omega \equiv n\cos\theta$ is conserved, so that equating $n\cos\theta$ at the point of emission to $n\cos\theta$ at the edge, where $n = 1$, gives $[(n\cos\theta)_{source}]^{-1} = u = [(\cos\theta)_{edge}]^{-1} > 1$, requiring particles to move faster than the speed of light. The situation improves somewhat for toroidal geometry. In a steady state with azimuthal symmetry, the two constants along the ray are[14] $k_\phi R = k_\phi R_o(1 + r/R_o\cos\theta)$, and ω (R_o is the

major radius; ϕ and θ toroidal and poloidal angles, and r the usual radial coordinate). Approximating $k_\phi = k\cos\theta$, the condition for the radiation to escape becomes

$$n\cos\theta\ (1 + r/R_o\cos\theta)\Big|_{source} = \cos\theta\ (1 + a/R_o\cos\theta)\Big|_{edge}$$

(a is the minor radius) so that, neglecting (r/R_o), the weakest escape condition is

$$\left(\frac{1}{n\cos\theta}\right)_{source} \geq \frac{1}{(1+\frac{a}{R_o})} \simeq \frac{1}{1.2} \simeq 0.8,$$

when $a/R_o \simeq 0.2$, as in TFR and Alcator. Note though, that $[n\cos\theta]^{-1}$ is just $u(\omega, \cos\theta)$, as plotted in figure 1, which thus shows that for typical parameters this weak escape condition is satisfied over most of the Cerenkov emission region, and also just above ω_p, where all the nonlinear emission occurs. Including the factor $(\cos\theta)_{edge}$ implies that to allow the escape of radiation from, for example, Cerenkov emitting particles with velocities above 0.9c, $\theta_{edge} \leq 30°$, which is not very restrictive. Even if a more detailed ray tracing analysis were to show that a significant fraction of radiation could not escape directly, it might still escape by scattering off density fluctuations. This would amplify some emission (being analogous to partial reflections) and could also alter the spectral shape. In the following, the lower limit to the velocity of the emitting particles is taken as 0.8 c, consistent with the weak escape condition. Furthermore, most of the emission is due to relativistic particles, for which the escape condition is not very restrictive.

To compute F^x, a uniform, cylindrical model is adopted, where the runaways are confined to a radius ℓ in a Tokamak of minor radius a. The walls are considered not to be smooth and, for simplicity, the radiation is assumed to be isotropized by reflection. The quantity q is defined as the fraction of radiation reflected back into the same mode, the remainder being absorbed or (a fraction p) converted to the other polarization. The energy emitted per second is S^x times the volume occupied by the runaways. This is isotropized, on reflection, over the area of the chamber walls and 2π solid angle. The total flux in one direction (2π solid angle) is then: (S^x)(source volume)/(area of chamber walls) = $S^x\ell^2/2a$. Including reflections and polarization scrambling[4], the result is:

$$F^x = \frac{q}{(1-q)} \frac{S^x \ell^2}{[1-(p/1-q)^2]} \left(\frac{1}{2a}\right) . \tag{9a}$$

The corresponding o mode flux is:

$$F^o = \frac{p}{(1-q)} F^x . \tag{9b}$$

C. Runaway Current

In many cases, $F^x(\omega)$ is approximately proportional to I_R, the current carried by the runaways. The runaway current satisfies:

$$I_R \alpha \int u f_T(u)\, du, \tag{10}$$

while the radiation flux satisfies:

$$F^x(\omega) \alpha \int \frac{d\varepsilon}{dt}(u,\omega) f_T(u)\, du. \tag{11}$$

These are approximately proportional when most of the current and radiative flux is produced by highly relativistic runaways. This is true because $d\varepsilon/dt\ (u,\omega)$ is a weak function of u near u = 1; the degree of weakness varies

with (Ω/ω_p). The integrals (10) and (11) may then be expanded, taking $u \equiv 1 - \delta$, in the form (u_R is the runaway velocity):

$$\int_{u_R}^{u_c} g(u)\ f_T(u)du = \int_{\delta_c}^{\delta_R} \left[g(1) - \delta \left.\frac{dg}{du}\right|_{u=1} + \cdots \right] f_T\,(1-\delta)d\delta\ . \qquad (12)$$

With this expansion, F^x and I_R are, to lowest order, both proportional to

$$\int_{\delta_c}^{\delta_R} f_T(1-\delta)d\delta,$$

the number density of relativistic runaways.

In the distribution used later, for example, $f_T(p)$ is flat in momentum space, and rapidly rising in velocity space, so that the velocities of most of the emitting particles are near the cutoff velocity. In figures 2 and 3, for example, $u_c = 0.97$, and $d\varepsilon/dt(u,\omega)$ varies by less than ten percent for $u > 0.9$.

When the exact Cerenkov spectrum (6) (convoluted with the detector response, as in figures 2 and 3) is reasonably similar to the observed spectrum in some frequency interval, from ω_1 to $\omega_2 = \omega_1 + \Delta\omega$, say, the Cerenkov mechanism may account for the emission in that interval. If, in addition, the conditions for equation (12) are satisfied, (12) can be used to relate I_R to F^x_{OBS}, the observed emission flux. Averaging over the region of fit, this relation is of the form:

$$I_R = C \left\langle F^x_{OBS} \Big/ \frac{d\varepsilon}{dt}(1,\omega) \right\rangle \equiv \frac{C}{\Delta\omega} \int_{\omega_1}^{\omega_2} d\omega \left(\frac{F^x_{OBS}(\omega)}{\frac{d\varepsilon}{dt}(1,\omega)} \right), \qquad (13)$$

where C is a constant depending on plasma and model parameters. This is

a very useful relation; although I_R can be computed once $f_T(u)$ is known, a theoretical runaway distribution such as (18), given later, is exponentially sensitive in n_T (where n_T is the runaway tail height) and u_c to plasma parameters (density, temperature, and applied electric field) which are only approximately known. The sensitivity is such that a ten percent uncertainty in line average density, electron temperature, and loop voltage (near one volt) causes the predicted classical value of (n_T/n) to vary by as much as two orders of magnitude.

To complete the Cerenkov emission model, C is computed, and F^x is normalized to F_{BB} (the blackbody flux for the electron temperature T_e), for convenience, and because the uncertainty in the absolute level of emission is sometimes substantial. From equations (6), (9), and (12),

$$F^x \approx \left(\frac{q\ell^2}{4(1-q)ac}\right)\left(\frac{\omega_p e^2}{[1-(^p/1-q)^2]}\right)\left(\int_{u_R}^{u_c} f_T(u)du\right)\delta_\omega , \tag{14}$$

where $\delta_\omega \equiv (2c/\omega_p e^2)d\varepsilon/dt(1,\omega)$ is the dimensionless spectral shape which is of order one. The blackbody flux in one direction and for one polarization is:

$$F_{BB} = \frac{\omega^2 T_e}{4\pi^2 c^2} . \tag{15}$$

The runaway current, using (12), is:

$$I_R = \left(\int_{u_R}^{u_c} f_T(u)du\right)\pi\ell^2 ec . \tag{16}$$

Both F^x and I_R are proportional to ℓ^2, the square of the runaway channel width, so that somewhat arbitrary quantity drops out of the result. Combining

(14), (15), and (16), the runaway current determined by the observed emission is then (where $v_e = (T_e/m_e)^{1/2}$):

$$I_R = \left\langle \left(\frac{F^x}{F_{BB}}\right)\left(\frac{\omega}{\omega_p}\right)^2 \left(\frac{1}{\delta\omega}\right) \right\rangle \frac{4(1-q)\left[1-\left(\frac{p}{1-q}\right)^2\right]}{q} \left(\frac{a\, v_e}{\omega_p}\right) nev_e. \quad (17)$$

While Equation (17) applies for all distributions, $f_T(u)$, that give a good spectral fit, and that allow use of equation (12), a specific distribution must, of course, be chosen for computation of the spectral shape. The one used here, and referred to in the following sections, is a flat tail in momentum space: $f_T(p) = (n_T/p_e)[H(p-p_R) - H(p-p_c)]$, where n_T is the tail height, and p_e, p_R, and p_c are the thermal, runaway, and cutoff momenta, respectively. This is an excellent approximation to the distribution function calculated in Ref. 11. Since $f_T(u)\, du = f_T(p)\, dp$,

$$f_T(u) = \left(\frac{n_T}{u_e}\right) [H(u-u_R) - H(u-u_c)]\, (1-u^2)^{-3/2}. \quad (18)$$

With this distribution, the emission integral (6) consists of elliptic integrals, and must be evaluated numerically. In the integration, equation (4) is numerically checked in each u interval, to determine which roots (3) contribute to the emission. In addition, regions where cyclotron absorption is significant are excluded, according to the usual condition:[15]

$$\frac{|\omega-\Omega|}{k\cos\theta_{\pm}} \leq 3v_e .$$

III. NONLINEAR EMISSION

A. Character of the Emission

The nonlinear emission mechanism consists of two incoherent wave-wave processes. One process, electromagnetic radiation from the scattering of a superthermal level of plasma oscillations with a thermal level of ion-acoustic fluctuations, was discussed in Ref. 9, and is referred to here as the scattering process. Another process, not included in Ref. 9, is the decay of plasma oscillations into ion-acoustic fluctuations and electromagnetic radiation, the decay process. For the hot plasmas ($T_e \sim$ 1keV.) considered here, the nonlinear emission, like the Cerenkov emission, occurs only for $\omega > \omega_p$. More precisely, $\omega > \omega_p$ unless the sound frequency $\omega_A \simeq |k_{A_\parallel} c_s| > (3/2)\omega_p (k_p/k_D)^2$, where $k_{A_\parallel}$ is the parallel acoustic wavenumber, $c_s \simeq (T_e/m_i)^{1/2}$ is the sound velocity, m_i is the ion mass, k_p is the plasma wavenumber, and k_D is the Debye wavenumber. For $k_p \simeq k_{A_\parallel} \simeq \omega_p/c$, this requires $(v_e/c) < (m_e/m_i)^{1/2}$, or $T_e \lesssim 0.3$ keV.

The decay process is analyzed much the same as the scattering process is in Ref. 9, but causes important qualitative differences in the resulting emission. The wave-kinetic equation is a continuity equation for the electromagnetic energy density: $\partial \varepsilon_{\underset{\sim}{k}}/\partial t + \underset{\sim}{\nabla} \cdot (\underset{\sim}{v}_g \varepsilon_{\underset{\sim}{k}}) =$ (sources) + (sinks), where $\varepsilon_{\underset{\sim}{k}}$ is the total (field plus particle) energy density per unit k-space volume and $\underset{\sim}{v}_g(\underset{\sim}{k})$ is the group velocity. For weakly damped modes, $k = k(\omega, \cos\theta)$, and $\varepsilon_{\underset{\sim}{k}}$ and other $\underset{\sim}{k}$ - dependent quantities can be regarded as functions of ω and $\cos\theta$. One source term is the Cerenkov emission, while the remaining sources and sinks are wave-wave scattering and decay terms. In steady-state, and when the spatial dependence of

$\underset{\sim}{v}_g$ can be neglected, the kinetic equation becomes:[16]

$$\underset{\sim}{v}_g \cdot \underset{\sim}{\nabla}\, \varepsilon_{\underset{\sim}{k}} = (4\pi)^4 \int d\underset{\sim}{k}_p \int d\underset{\sim}{k}_A \left\{ |\mu^S|^2 \left[\frac{\delta(\underset{\sim}{k}-\underset{\sim}{k}_p-\underset{\sim}{k}_A)\ \delta(\omega_{\underset{\sim}{k}}-\omega_{\underset{\sim}{k}_p}-\omega_{\underset{\sim}{k}_A})}{\omega \frac{\partial\varepsilon}{\partial\omega}\ \omega_p \frac{\partial\varepsilon_p}{\partial\omega_p}\ \omega_A \frac{\partial\varepsilon_A}{\partial\omega_A}} \right] \right.$$

$$\times \left[\varepsilon_{\underset{\sim}{k}_p} \varepsilon_{\underset{\sim}{k}_A} - \frac{\omega_A}{\omega} \varepsilon_{\underset{\sim}{k}} \varepsilon_{\underset{\sim}{k}_p} - \frac{\omega_p}{\omega} \varepsilon_{\underset{\sim}{k}} \varepsilon_{\underset{\sim}{k}_A} \right] +$$

$$\left. |\mu^D|^2 \left[\frac{\delta(\underset{\sim}{k}-\underset{\sim}{k}_p+\underset{\sim}{k}_A)\ \delta(\omega_{\underset{\sim}{k}}-\omega_{\underset{\sim}{k}_p}+\omega_{\underset{\sim}{k}_A})}{\omega\frac{\partial\varepsilon}{\partial\omega}\ \omega_p \frac{\partial\varepsilon_p}{\partial\omega_p}\ \omega_A \frac{\partial\varepsilon_A}{\partial\omega_A}} \right] \left[\varepsilon_{\underset{\sim}{k}_p} \varepsilon_{\underset{\sim}{k}_A} + \frac{\omega_A}{\omega} \varepsilon_{\underset{\sim}{k}_p} \varepsilon_{\underset{\sim}{k}} - \frac{\omega_p}{\omega} \varepsilon_{\underset{\sim}{k}} \varepsilon_{\underset{\sim}{k}_A} \right] \right\}$$

$$+ P_{\underset{\sim}{k}}^{L}, \qquad (19)$$

where superscripts S and D refer to the scattering and decay processes, and subscripts A and p refer to acoustic and plasma waves. The quantities ε, ε_p, and ε_A are the dielectric constants for the transverse, plasma, and acoustic waves. The first term on the right hand side of (19) was discussed in Ref. 9. The second term consists of two emission terms, corresponding to the induced decay of plasma waves by transverse and acoustic waves, and one absorption term, corresponding to the scattering of transverse with acoustic waves to produce plasma oscillations. An additional index, denoting whether emission is in the ordinary or extraordinary mode, is understood. The quantity μ is the non-linear coupling coefficient, defined such that the scattering of two waves produces a non-linear current along the polarization of a third, emitted wave:

$$J^{NL}_{\underset{\sim}{k}_3},\ \underset{\sim}{k}_3 = \underset{\sim}{k}_1 + \underset{\sim}{k}_2,\ \omega_3 = \omega_1 + \omega_2 = \int d^3\underset{\sim}{k}_1 \int d\omega_1\, \mu(\underset{\sim}{k}_1, \underset{\sim}{k}_2, \omega_1, \omega_2) E_{\underset{\sim}{k}_1, \omega_1}\ E_{\underset{\sim}{k}_2, \omega_2}.$$

The Cerenkov source term, $P^L_{\underset{\sim}{k}}$, contributes only to the x mode.

The electrostatic turbulence produced by the runaways, $\varepsilon_{\underset{\sim}{k}_p}$, has been calculated in Ref. 11 by requiring a steady state electron distribution function, where the force of the applied electric field is balanced by an effective friction due to pitch-angle scattering by the turbulence. The unmagnetized plasma oscillations are greatest at the frequency corresponding to the central density. This is because the runaways are cut off by magnetized plasma oscillations, which grow as they convect out of the plasma. Similarly, the waves are in a state of marginal stability, where collisional damping is balanced by Landau growth due to a small positive slope in the distribution function. The level of plasma oscillations found in Ref. 11 is so much greater than the thermal level acoustic fluctuations ($\varepsilon_{\underset{\sim}{k}_p}/\varepsilon_{\underset{\sim}{k}_A} \sim 10^{10}$) that $(\varepsilon_{\underset{\sim}{k}_p}/\varepsilon_{\underset{\sim}{k}_A}) \gg (\omega_p/\omega_A)$, and an excellent approximation to (19) is:

$$\underset{\sim}{v}_g(\underset{\sim}{k}) \cdot \underset{\sim}{\nabla}\, \varepsilon_{\underset{\sim}{k}} = (\gamma_{\underset{\sim}{k}}^D - \gamma_{\underset{\sim}{k}}^S)\, \varepsilon_{\underset{\sim}{k}} + \left(\frac{\omega}{\omega_A}\gamma_{\underset{\sim}{k}}\, \varepsilon_{\underset{\sim}{k}_A}\right)^D + \left(\frac{\omega}{\omega_A}\gamma_{\underset{\sim}{k}}\, \varepsilon_{\underset{\sim}{k}_A}\right)^S + P^L_{\underset{\sim}{k}}. \tag{20}$$

Here, $\gamma^D_{\underset{\sim}{k}}$ is the induced radiation amplification rate, and $\gamma^S_{\underset{\sim}{k}}$ is the induced damping rate. They are given by:

$$\gamma^{D,S}_{\underset{\sim}{k}} =$$

$$(4\pi)^4 \int d^3k_p \int d^3k_A \left[\frac{|\mu^{D,S}|^2}{\omega \frac{\partial \varepsilon}{\partial \omega}\, \omega_p \frac{\partial \varepsilon_p}{\partial \omega_p}\, \omega_A \frac{\partial \varepsilon_A}{\partial \omega_A}}\right] \delta(\underset{\sim}{k}-\underset{\sim}{k}_p \pm \underset{\sim}{k}_A)\, \delta(\omega - \omega_{\underset{\sim}{k}_p} \pm \omega_{\underset{\sim}{k}_A}) \left(\frac{\omega_{\underset{\sim}{k}_A}}{\omega}\right) \varepsilon_{\underset{\sim}{k}_p}, \tag{21}$$

where D corresponds to the upper sign, and S the lower sign. In the following sections, where estimates of the nonlinear emission are made,

the distinction between the scattering and decay processes actually is not important. This is, however, a special case, and in general, when, for example, the acoustic wave level is elevated enough to generate significant nonlinear emission, the distinction can be very important. Thus, before estimating the nonlinear emission, general formulas distinguishing the scattering and decay processes are here given. The delta functions in γ impose the matching conditions, and already contain the dispersion relations. This is enough to determine $\underset{\sim}{k}_p$ and $\underset{\sim}{k}_A$ as functions of ω and $\cos\theta$, so that, after doing the $\underset{\sim}{k}$ integrals, the $\underset{\sim}{k}$ vectors where everything is evaluated are denoted by $\underset{\sim}{k}_{p,A}^{D,S}(\omega,\cos\theta)$. Converting the delta function of $\omega_p(\underset{\sim}{k}_p)$ to a function of $\underset{\sim}{k}_p$, noting that $\varepsilon_{\underset{\sim}{k}_p}$ is proportional to $\delta(\underset{\sim}{k}_{p_\perp})$, the γ's become (super-scripted expressions with D and S are evaluated at $\underset{\sim}{k}_{p,A}^{D,S}$):

$$\gamma_{\underset{\sim}{k}}^{D,S} = \frac{(4\pi)^4 |\mu^{D,S}|^2}{\left(\omega \frac{\partial\varepsilon}{\partial\omega}\omega_p \frac{\partial\varepsilon_p}{\partial\omega_p}\omega_A \frac{\partial\varepsilon_A}{\partial\omega_A}\right)^{D,S}} - \frac{\left(\frac{\omega_{\underset{\sim}{k}_A}^{D,S}}{\omega}\right)\varepsilon_{\underset{\sim}{k}_p}^{D,S}}{|v_g^P - v_g^A|_{\parallel}^{D,S}} . \qquad (22)$$

Equation (20) can then be put in a more useful form:

$$\frac{d\varepsilon_{\underset{\sim}{k}}}{ds} = \frac{-\varepsilon_{\underset{\sim}{k}}\chi}{\ell} + \frac{P_{\underset{\sim}{k}}}{v_g} , \qquad (23)$$

where $P_{\underset{\sim}{k}}$ is the last three terms on the right hand side of equation (20), $\chi \equiv \ell(\gamma_{\underset{\sim}{k}}^S - \gamma_{\underset{\sim}{k}}^D)/v_g$, and s is the distance along the ray.

Equation (23) is valid inside the runaway channel; wave-particle effects have been neglected, for the x mode, as described above, and for the o mode, whose phase velocity is greater than the speed of light. At the edge of the runaway channel, for group velocity angle θ_g, $\varepsilon_{\underset{\sim}{k}}$ is:

$$\varepsilon_{\underset{\sim}{k}}\left(\frac{\ell}{\sin\theta_g}\right) = \frac{P_{\underset{\sim}{k}}\ell}{v_g \sin\theta_g} \frac{[1 - \exp(-\chi/\sin\theta_g)]}{(\chi/\sin\theta_g)} \tag{24}$$

which simplifies in two cases. In the "optically thick" case, defined by $|\chi/\sin\theta_g| > |\chi| >> 1$, $\varepsilon_{\underset{\sim}{k}}(\ell/\sin\theta_g) = (P_{\underset{\sim}{k}}\ell/\chi v_g) = P_{\underset{\sim}{k}}/(\gamma^S_{\underset{\sim}{k}} - \gamma^D_{\underset{\sim}{k}})$, when $\chi > 0$, and the emission is damped; when $\chi < 0$, and the emission is amplified, $\varepsilon_{\underset{\sim}{k}}(\ell/\sin\theta_g) = (P_{\underset{\sim}{k}}/|\gamma^S_{\underset{\sim}{k}} - \gamma^D_{\underset{\sim}{k}}|)\exp(|\chi|/\sin\theta_g)$. In the optically thin case, $\chi < \chi/\sin\theta_g << 1$, and $\varepsilon_{\underset{\sim}{k}}(\ell/\sin\theta_g) = (P_{\underset{\sim}{k}}\ell/v_g\sin\theta_g)$. Note that the meanings of "thick" and "thin" are complicated by the fact that two wave-wave processes are present. The thickness is determined by a difference of growth rates, $\chi \alpha \gamma^S - \gamma^D$, while the source strength goes as the sum, $P_{\underset{\sim}{k}} \alpha \gamma^S + \gamma^D$. If, for example, γ^S and γ^D are both large but cancel substantially, the emission can be "thin", yet large compared to the blackbody level. Unlike the result in Ref. 9, in such a case the emission is not only superthermal, but also sensitive to the plasma parameters through $P_{\underset{\sim}{k}}$.

B. Detailed Formulas

The quantities $\varepsilon_{\underset{\sim}{k}_p}$, $\varepsilon_{\underset{\sim}{k}_A}$, γ^D, γ^S, and thus the quantities in Eq. (22), and v_g must be found to determine the level of emission and its sensitivity to variation in the plasma parameters, both as functions of ω and θ. For $\varepsilon_{\underset{\sim}{k}_p}$ the spectrum used is given in Ref. 11 as (subscripts $\|$ and $\perp$

denote components parallel and perpendicular to the magnetic field):

$$\varepsilon_{\underset{\sim}{k}_p} = \varepsilon_{k_{p_\parallel}} = \left(\frac{E}{E_R}\right) n_T \left(\frac{T_e}{2}\right) \left(\frac{1}{k_D}\right) \left(\frac{k_D}{k_{p_\parallel}}\right)^3, \tag{25}$$

for $k_{p_\parallel} > (\omega_p/c)$; ε_{k_p} is zero for $k_{p_\parallel} < (\omega_p/c)$, or $k_{p_\perp} \neq 0$. Here, E_R is the runaway field: $E_R = [4\pi ne^3 \ell n(\Lambda)/T_e]$, and $\ell n(\Lambda)$ is the Coulomb logarithm. For the acoustic wave, a thermal level corresponding to the ion temperature T_i is taken[17]:

$$\varepsilon_{\underset{\sim}{k}_A} = \frac{T_i}{(2\pi)^3} . \tag{26}$$

To get $k_{P,A}^{S,D}$ the dispersion relations, including (1), are combined with the matching conditions: $\omega = \omega_p \pm \omega_A$, $k_\parallel = k_p \pm k_{A_\parallel}$, and $k_\perp = \pm k_{A_\perp}$, plus corresponding to scattering, and minus to decay. The remaining dispersion relations are $\omega_{\underset{\sim}{k}_A} = |k_{A_\parallel}| c_s$, where $c_s = [(T_e + 3T_i)/m_i]^{1/2}$, and $\omega_p = \omega_{pe}\,[1 + (3/2)(k_p^2/k_D^2)]$. Here, and in the remainder of section III., the subscript p refers to the plasma wave, while ω_{pe} is the local electron plasma frequency. Since $\omega_A \ll \omega_{pe}$, $\Delta \equiv (\omega - \omega_{pe})/\omega_{pe} \ll 1$ can be used as a convenient expansion parameter. Parallel k matching can be rewritten as $|k_{a_\parallel}| = (k_p - k\cos\theta)\,\mathrm{sgn}(k_p - k\cos\theta)$ which, substituted in the ω matching condition, along with the dispersion relations, yields a quadratic equation for $k_p^{S,D}(\omega,\cos\theta)$. The solution is, defining $\alpha_p^{S,D}(\omega,\cos\theta) \equiv (c/\omega_{pe}) k_p^{S,D}(\omega,\cos\theta)$:

$$\alpha_p^{S,D}(\Delta,\cos\theta) =$$

$$\frac{\mp\left(\frac{c_s}{c}\right)\Sigma + \left\{\left(\frac{c_s}{c}\right)^2 + 6\left(\frac{v_e}{c}\right)^2\left[\Delta \pm (1+\Delta)\left(\frac{c_s}{c}\right)\cos\theta \times n(\Delta,\cos\theta)\Sigma\right]\right\}^{1/2}}{3\left(\frac{v_e}{c}\right)^2}, \qquad (27)$$

where S and D correspond to upper and lower signs respectively, and $\Sigma \equiv \text{sgn}\,[\alpha_p - n(1+\Delta)\cos\theta]$. In practice, only one value of Σ gives a consistent solution. (There is also a small region where there is no consistent sign, and therefore no matching). The plus sign has been chosen in the root of the quadratic because (for $T_e \simeq 1$ keV.) for values of Δ such that $\alpha > 1$, when there is matching to the superthermal plasma wave spectrum, the radical is greater than (c_s/c). Given α_p, $k_A^{S,D}$ follows from k matching.

To compute the coupling coefficients μ, the polarizations of the electromagnetic waves are needed. For scattering, this is the polarization of the electromagnetic mode. For decay, the coupling is the same as for the inverse process, where electromagnetic and acoustic waves scatter to produce plasma oscillations, whose polarization is along the magnetic field. The electromagnetic polarization in the high frequency, cold plasma limit is:

$$\hat{\underline{\pi}} = \frac{\left[\hat{\underline{x}} + \left(\frac{i\varepsilon_2}{(n^2-\varepsilon_1)}\right)\hat{\underline{y}} + \left(\frac{n^2\sin\theta\cos\theta}{n^2\sin^2\theta-\varepsilon_3}\right)\hat{\underline{z}}\right]}{\left[1 + \frac{\varepsilon_2^2}{(n^2-\varepsilon_1)^2} + \frac{n^4\sin^2\theta\cos^2\theta}{(n^2\sin^2\theta-\varepsilon_3)^2}\right]^{1/2}}, \qquad (28)$$

where $\hat{B} = \hat{z}$. Expanding in $(\varepsilon_3/\sin^2\theta)$ (which is small except at very small angles, where the polarizations become right and left circularly polarized, and the coupling becomes small) the lowest order polarizations for the two modes are

$$\hat{\pi}_x(\cos\theta,\omega) = \frac{\left[\hat{x} - i\left(\frac{\Omega}{\omega_{pe}}\right)\hat{y} + \frac{\cos\theta}{\sin\theta}\hat{z}\right]}{\left[\frac{1}{\sin^2\theta} - \left(\frac{\Omega}{\omega_{pe}}\right)^2\right]^{1/2}}$$

and $\hat{\pi}_o = \hat{z}$. To compute μ, these polarizations are dotted into the total nonlinear current of the two scattering waves (denoted by 1 and 2). This total current is of the form $(n_o + \tilde{n}_1 + \tilde{n}_2 + \cdots)(\tilde{v}_1 + \tilde{v}_2 + \tilde{v}_{NL} + \cdots)$, and the part which satisfies matching is $\tilde{n}_1\tilde{v}_2 + \tilde{n}_2\tilde{v}_1 + n_o\tilde{v}_{NL} + \cdots$. To compute this current, the ions are treated in the guiding center approximation. This assumption, $\omega_A \ll \Omega_i$ (the ion cyclotron frequency) is also used to get the magnetized ion-acoustic dispersion relation. It is justified for o mode emission because $k_o \ll (\omega_{pe}/c)$, so that k_A is nearly anti-parallel to k_p and B, and magnetic effects can be neglected. For the x mode, first note that the coupling is proportional to $(\hat{\pi}_x \cdot \hat{z}/k_A)^2$ (provided $J_x^{NL} \cdot \hat{z} \gg J_x^{NL} \cdot (\hat{x}, \hat{y})$, as shown later for the nonlinear current J^{NL}). This factor is of order one at small and intermediate angles, but $\lesssim 10^{-1}$ for $\theta > 60°$ (taking $\Omega/\omega_{pe} \simeq 3$). But, $\omega_A \simeq 2\sin^2(\theta/2)(c_s/c)\omega_{pe} \lesssim (\Omega_i/3)$, for $\theta < 60°$, so that the guiding center approximation is good in the region of strong coupling to the x mode. The fluid equations may then be used to compute $\mu = (\hat{\pi} \cdot J^{NL}_{k_1+k_2,\omega_1+\omega_2}/E_{k_1,\omega_1}E_{k_2,\omega_2})$. The equation of continuity shows that for scattering, $(\tilde{n}_A\tilde{v}_p/\tilde{n}_p\tilde{v}_A) \simeq (c/c_s) \gg 1$, and for decay as well, $(\tilde{n}_A\tilde{v}_{x,o}/\tilde{n}_{x,o}\tilde{v}_A) \simeq (c/c_s)$. Thus, $\hat{\pi} \cdot J^{NL} \simeq (\hat{\pi} \cdot \hat{z})J^{NL}$ for both

processes, since $\underset{\sim}{v}_p = v_p\hat{z}$ dominates the nonlinear current for the scattering process, and for the decay since the polarization is the same as that of the plasma oscillations, along the magnetic field. The resulting coefficients are:

$$\mu_x^S = \hat{\pi}_x \cdot \hat{z}\left(\frac{-\omega_{pe}q}{4\pi k_A T_e}\right) \simeq \frac{\cos\theta}{[1 + \sin^2\theta(\frac{\Omega}{\omega_{pe}})^2]1/2}\left(\frac{-\omega_{pe}q}{4\pi k_A T_e}\right), \tag{29a}$$

$$\mu_o^S = \left(\frac{-\omega_{pe}q}{4\pi k_A T_e}\right), \tag{29b}$$

$$\mu_x^D = \hat{\pi}_x \cdot \hat{z}\left(\frac{-\omega_{pe}q}{4\pi k_A T_e}\right)\left(\frac{\omega_{pe}}{\omega}\right) \simeq \frac{\cos\theta}{[1 + \sin^2\theta(\frac{\Omega}{\omega_{pe}})^2]1/2}\left(\frac{-\omega_{pe}q}{4\pi k_A T_e}\right)\left(\frac{\omega_{pe}}{\omega}\right), \tag{29c}$$

$$\mu_o^D = \left(\frac{-\omega_{pe}q}{4\pi k_A T_e}\right)\left(\frac{\omega_{pe}}{\omega}\right). \tag{29d}$$

The remaining pieces of χ and $P_{\underline{k}}$ to compute are the $\omega(\partial\varepsilon/\partial\omega)$'s, and the group velocities. The quantity $\omega(\partial\varepsilon/\partial\omega)$ is almost exactly two for the plasma and electromagnetic waves. For the acoustic wave, $\omega_A(\partial\varepsilon/\partial\omega_A) = 2(k_D/k_A)^2$. The group velocities are $v_{gp} = (d\omega_p/dk_p) = 3(v_e/c)v_e\alpha$, and $v_{g_{\|}A} = \partial\omega_A/\partial k_{A_{\|}} = c_s\,\mathrm{sgn}(k_{A_{\|}})$, for the plasma and acoustic waves. To first order in $(\varepsilon_3/\sin^2\theta)$, the magnitude and direction of the x mode group velocity are:

$$v_{gx} = \left(\frac{c_{nx}}{\frac{1}{\sin^2\theta} + 2\left(\frac{\omega}{\Omega}\right)^2 - \left(\frac{\omega_{pe}}{\Omega}\right)^2}\right) \tag{30a}$$

and

$$\tan(\theta_{gx} - \theta) = \frac{\varepsilon_3\cos\theta}{n_x^2\sin^3\theta}. \tag{30b}$$

For the o mode:

$$v_{go} = n_o c \sin\theta \tag{31a}$$

and

$$\tan(\theta_{go} - \theta) = \cot\theta. \tag{31b}$$

C. Integrated Emission of x Mode

The nonlinear emission near ω_{pe} can, in principle, be detected either directly, or after the radiation has been reflected. Since direct emission must be nearly perpendicular to the magnetic field, the coupling to the x mode is suppressed by at least three and a half orders of magnitude; this follows for $\theta \geq 88°$, $(\Omega/\omega_{pe}) \geq 2$, and noting that the group and phase velocity angles are approximately equal near perpendicular emission. Only reflected x emission is then significant. To estimate this emission, first note that $(P_{\underset{\sim}{k}}\ell/v_g \sin\theta_g)$ is an upper limit to $\varepsilon_{\underset{\sim}{k}}$. This will be used to show that with a termal level of sound fluctuations the emission is negligible.

The rate at which energy leaves a length L of the runaway channel (analogous to $S^x V$ for the Cerenkov emission) is

$$2\pi\ell L \int d^3\underset{\sim}{k}\varepsilon_{\underset{\sim}{k}} v_g \sin\theta_g.$$

Converting this to a reflected and isotropized flux, as for the Cerenkov emission, gives:

$$F^{x,NL} = \frac{q\ell}{a(1-q)} \frac{1}{[1-(\frac{p}{1-q})^2]} \int d^3\underset{\sim}{k}\varepsilon_{\underset{\sim}{k}} v_g \sin\theta_g. \tag{32}$$

The units of $F^{x,NL}$ are erg./cm.^{2}-sec.; since the predicted nonlinear

spectral shape is a line much narrower than the resolution of the observations, the frequency-integrated emission has been computed for comparison. Substituting $\varepsilon_{\underset{\sim}{k}} = (P_{\underset{\sim}{k}} \ell / v_g \sin\theta_g)$, and rewriting $d^3\underset{\sim}{k} = 2\pi d(\cos\theta) k^2 dk = 2\pi d(\cos\theta) k^2 (\partial k/\partial\omega)(\partial\omega/\partial\alpha_p) d\alpha_p$,

$$F^{x,NL} = \frac{2\pi\ell^2}{a} \frac{q}{(1-q)[1-(\frac{p}{1-q})^2]} \iint d(\cos\theta) d\alpha_p \, k^2 (\alpha_p, \cos\theta) \frac{\partial k}{\partial\omega} \frac{\partial\omega}{\partial\alpha_p} P_{\underset{\sim}{k}} . \qquad (33)$$

As previously mentioned, emission is negligible at small angles, $\sin^2\theta \leq \varepsilon_3 << 1$, since the polarization becomes perpendicular to the magnetic field. Thus the only significant contribution to (33), and all following integrals, comes from the region where $\sin^2\theta >> \varepsilon_3$. In that limit,

$$(\frac{\partial k}{\partial\omega})_x \approx \frac{1}{c} \left[1 + \cot^2\theta + \left(\frac{\omega_{pe}}{\Omega}\right)^2\right]$$

and

$$(\frac{\partial\omega}{\partial\alpha_p}) = 3\left(\frac{v_e}{c}\right)^2 \omega_{pe} \alpha .$$

Furthermore, $P_{\underset{\sim}{k}} \approx 2(\omega/\omega_A)\varepsilon_{\underset{\sim}{k}_A} \gamma^S_{\underset{\sim}{k}}$, and (c_s/v_e) can be neglected compared to $3(v_e/c)$. With these approximations, the resulting flux, normalized to F_{BB}, the blackbody level integrated over the observed width of the ω_{pe} peak, is:

$$\frac{F^{x,NL}}{F_{BB}} = \left(\frac{\pi}{4}\right)\left(\frac{c}{v_e}\right)^2\left(\frac{\omega_{pe}}{\delta\omega}\right)\left(\frac{\ell}{a}\right) \frac{q\,(\omega_{pe}\ell/c)}{(1-q)\,[1-(\frac{p}{1-q})^2]} \left(\frac{T_i}{T_e}\right)\left(\frac{E}{E_R}\right) \times$$

$$\left(\frac{n_T}{n}\right) \frac{[1 - \alpha_{max}^{-2}]}{[1 + \delta\omega/\omega_{pe}]} \; f(\eta,\psi). \qquad (34)$$

Here, $\delta\omega$ is the width of the observed ω_{pe} peak, equated here to the

resolution of the detector, so that $F_{BB} = (T_e\omega_{pe}^3/2\pi^2c^2)(\delta\omega/\omega_{pe})(1+\delta\omega/\omega_{pe})$. The parameter $\eta \equiv (\Omega/\omega_{pe})_o$, and ψ is the cosine of the minimum angle for which $(\varepsilon_3/\sin^2\theta) << 1$, taken here as eight degrees, corresponding to $(\omega/\omega_{pe}) \simeq 1.001$. The maximum value of α_p is $\alpha_{max} \simeq 3$, estimated from (27), taking $(k_{A_{||}})_{max} = k_D$, which gives Δ a maximum of $(k_D c_s/\omega_{pe}) \simeq 0.02$. The function $f(\eta,\psi)$ which is of order one, comes from the θ integral, and is:

$$f(\eta,\psi) \equiv \frac{-2\psi}{\eta^4} + \left(\frac{1}{\eta^2-1}\right)\left[\left(1+\frac{1}{\eta^2}\right)^{3/2}\ell n\left|\frac{(1+\eta^2)^{1/2}+\eta\psi}{(1+\eta^2)^{1/2}-\eta\psi}\right|\right] + \ell n\left|\frac{1+\psi}{1-\psi}\right| \quad . \tag{35}$$

The result given in (34) is constrained by the Cerenkov model for the broadband emission. In particular, to explain the broadband emission requires a tail height which can be obtained from equations (16), (17), and (18) (subscript C refers to the Cerenkov emission):

$$\left(\frac{n_T}{n}\right)_C = \left(\frac{4}{\pi}\right)\left(\frac{v_e}{c}\right)^2\left(\frac{av_e}{\ell^2\omega_{pe}}\right)\left(\frac{1-q}{q}\right)\left[1-\left(\frac{p}{1-q}\right)^2\right]\frac{\left\langle\left(\frac{F^x}{F_{BB}}\right)\left(\frac{\omega}{\omega_{pe}}\right)^2\frac{1}{\delta_\omega}\right\rangle}{[u_c\gamma_c - u_R\gamma_R]}, \tag{36}$$

where $\gamma = (1-u^2)^{-1/2}$. The question, then, is whether $F^{x,NL} \geq F_{BB}$, since the discrepancy between the Cerenkov emission and the observed ω_{pe} peak is comparable to F_{BB}. Substituting $(n_T/n)_C$ for (n_T/n) in Eq. (34) yields:

$$\frac{F^{x,NL}}{F_{BB}} = \left(\frac{\omega_{pe}}{\delta\omega}\right)\left(\frac{v_e}{c}\right)\left(\frac{T_i}{T_e}\right)\left(\frac{E}{E_R}\right)\frac{\left[1-\alpha_{max}^{-2}\right]}{(1+\delta\omega/\omega_{pe})}f(\eta,\psi)\frac{\left\langle\left(\frac{F^x}{F_{BB}}\right)\left(\frac{\omega}{\omega_{pe}}\right)^2\frac{1}{\delta_\omega}\right\rangle}{[u_c\gamma_c - u_R\gamma_R]}. \tag{37}$$

For figures 2 and 3, $(\omega_{pe}/\delta\omega) \simeq 4$, $(v_e/c) \simeq 1/22$, $(T_i/T_e) \simeq 1/3$, $(E/E_R) \simeq 1/20$, $\alpha_{max} \simeq 3$, $\eta \simeq 2$, $\psi \simeq 0.99$, $f(\eta,\psi) \simeq 2$, the frequency average of $[(F^x/F_{BB})(\omega/\omega_{pe})^2(1/\delta_\omega)] \simeq 5$, and $[u_c\gamma_c - u_R\gamma_R] \simeq 2.7$. For these values, $(F^{x,NL}/F_{BB}) \simeq 8 \times 10^{-3}$, which is certainly negligible.

This result is to be contrasted to that in Ref. 9 where it was found that $(F^{x,NL}/F_{BB}) \simeq 3$. There are three main reasons for this disagreement. First, the value of $(n_T/n)_C$ (for $\ell = 3$cm.) indicated here by the Cerenkov emission is much less than the value taken in Ref. 9. Second, $(\omega_{pe}/\delta\omega)$ is taken as 4 here, not 10 as in Ref. 9. Third, partly as a consequence of the first two factors, the emission is found here to be optically thin, not thick as in Ref. 9.

To see the contrast in results in more detail, the result in Ref. 9 can be compared with equation (34), giving (the values found in Ref. 9 are denoted by subscript HMY):

$$\frac{F^{x,NL}}{F_{BB}} = \left(\frac{\gamma\ell}{c}\right)_{HMY}\left(\frac{\ell}{a}\right)\left(\frac{q}{(1-q)\left[1-\left(\frac{p}{1-q}\right)^2\right]}\right)\frac{\left(\frac{n_T}{n}\right)_C}{\left(\frac{n_T}{n}\right)_{HMY}}\frac{f(\eta,\psi)}{[1+\delta\omega/\omega_{pe}]}$$

$$\times \left[1-\alpha_{max}^{-2}\right]\left(\frac{F^{x,NL}}{F_{BB}}\right)_{HMY} . \qquad (38)$$

The first factor is present because the emission is optically thin. An approximate upper limit to $(\chi_x/\sin\theta_g)$ is

$$\left(\frac{\pi}{12}\right)\left(\frac{\omega_{pe}\ell}{c}\right)\left(\frac{m_e}{m_i}\right)^{1/2}\left(\frac{c}{v_e}\right)^3\left(\frac{E}{E_R}\right)\left(\frac{n_T}{n}\right)\frac{\left|\alpha^S_{A_\parallel}\right|}{\left(\alpha^S_p\right)^4}\frac{\cot^2\theta}{[1+(\sin^2\theta)\eta^2]} .$$

Taking the paramaters following (33), and $(n_T/n)_{HMY} = 7.2 \times 10^{-4}$,

$\omega_{pe} \simeq 4 \times 10^{11}$Hz., and $\ell \simeq 3$ cm., the first six factors are about 10^{-1}. This is smaller than the result in Ref. 9 (where $\chi \simeq 1$ is found) mainly because Bohm-Gross dispersion has been correctly included, accounting for an additional factor of $(1/3)(m_e/m_i)^{1/2}(c/v_e) \simeq 1/6$. While the spectral shape is correspondingly broadened by the dispersion, so that the frequency-integrated emission is probably little altered, the transport of the radiation is much different. The plasma is transparent to emission so that computing the reflected, isotropized emission is appropriate. The emission is also proportional to ℓ, the distance over which the radiation is amplified. Regarding $\chi_x/\sin\theta_g$, the $\cot^2\theta$ factor may allow a small amount of optically thick emission for $\theta \lesssim 17°$, but this would only make the integrated emission somewhat smaller than in (33). The second and third factors in (34) correspond to geometric and reflection effects on the isotropized emission from a finite source. When $\ell = 3$ cm., $(n_T/n)_C = 5 \times 10^{-6}$, so that $(n_T/n)_C/(n_T/n)_{HMY}$ is about 7×10^{-3}. If ℓ is much smaller, this ratio increases, but is cancelled by the decrease in the first two factors. The remaining factors account for the x mode polarization and group velocity as functions of θ and ω.

D. Integrated Emission of o Mode

For the o mode, coupling is strong at perpendicular propagation, and unreflected emission can be detected. Direct emission is, in fact, greater than reflected emission, although both are small compared to the blackbody level, for $(n_T/n) = (n_T/n)_C$, and $\varepsilon_{k_A} = \dfrac{T_i}{(2\pi)^3}$.

To estimate the emission, consider, again for $\varepsilon_3 \ll \sin^2\theta$, $(\chi_o^S/\sin\theta_g)$, which is approximately equal to $(\ell\gamma^S/v_g)$, since $\sin\theta_g$ is one to first order in $(\varepsilon_3/\sin^2\theta)$. Then χ_o^S is easily found to be (note subscripts and superscripts "o" on χ, v_g, γ, and F denote the ordinary mode):

$$\chi_o^S = \left(\frac{m_e}{m_i}\right)^{1/2}\left(\frac{\pi}{12}\right)\left[\frac{\omega_{pe}\ell}{c\varepsilon_3^{1/2}}\right]\left(\frac{c}{v_e}\right)^3\left(\frac{E}{E_R}\right)\left(\frac{n_T}{n}\right)\frac{|\alpha_{A_\parallel}^S|}{(\alpha_p^S)^4}\,. \tag{39}$$

Substituting $(n_T/n)_C$ for (n_T/n), as before, gives:

$$\chi_o^S = \left(\frac{1}{3}\right)\left(\frac{m_e}{m_i}\right)^{1/2}\left(\frac{a}{\ell}\right)\left(\frac{E}{E_R}\right)\left(\frac{1}{\varepsilon_3^{1/2}}\right)\left(\frac{1-q}{q}\right)\left[1-\left(\frac{p}{1-q}\right)^2\right] \times \frac{\left\langle\left(\frac{F^x}{F_{BB}}\right)\left(\frac{\omega}{\omega_{pe}}\right)^2\left(\frac{1}{\delta\omega}\right)\right\rangle}{[u_c\gamma_c - u_R\gamma_R]}\frac{|\alpha_{A_\parallel}^S|}{(\alpha_p^S)^4}\,. \tag{40}$$

Estimating χ_o^S for figures 4 and 5, taking $|\alpha_{A_\parallel}^S|/(\alpha_p^S)^4$ of order one, $\chi_o^S = (5 \times 10^{-2}/\ell)$. Since $\chi_o = \chi_o^S - \chi_o^D$, this is an upper limit to χ_o, and, since $(\varepsilon_3)^{-1/2}$ has been evaluated at $\omega/\omega_{pe} \approx 1.001$, the emission will be thin for all frequencies, and all angles greater than about ten degrees. The possibility that ℓ is small enough to make the emission thick is unlikely, unless some mechanism is found to prevent runaway outside of a tiny central region; in the theory in Ref. 11 relativistic runaways are predicted out to three or more centimeters from the axis. Then, ε_k is approximately $2(\omega/\omega_A)\gamma_o^S[T_i/(2\pi)^3](\ell/v_g)$. Equating this to an effective thermal level, $T_{eff}/(2\pi)^3$, and substituting $(n_T/n)_C$

in the formula for γ_o^S,

$$T_{eff} = \left(\frac{2}{3}\right)\left(\frac{a}{\ell}\right)\left(\frac{1}{\epsilon_3^{1/2}}\right)\left(\frac{E}{E_R}\right)\left(\frac{1-q}{q}\right)\left[1 - \left(\frac{p}{1-q}\right)^2\right]$$

$$\times \left\langle \left(\frac{F^x}{F_{BB}}\right)\left(\frac{\omega}{\omega_{pe}}\right)^2\left(\frac{1}{\delta\omega}\right)\right\rangle \left(\frac{c}{v_e}\right)\left[\frac{T_i}{(u_c\gamma_c - u_R\gamma_R)\alpha_p^4}\right] . \qquad (41)$$

The energy density $\epsilon_{\underset{\sim}{k}}$ corresponds to emission that directly fills the entire detector acceptance region. With Alcator in mind, this region is approximately a cone of half-angle two degrees about the perpendicular to the magnetic field. The radiation emerges in a cone of half-angle 30° or larger. This follows from the conservation of k_ϕ:

$$\theta_{edge} = \cos^{-1}\left(\frac{\epsilon_3^{1/2}\cot\theta_{source}}{\left[1 + \left(\frac{a}{R_o}\right)\cos\theta\right]}\right) .$$

The detector is thus filled with rays corresponding to energy density $\epsilon_{\underset{\sim}{k}} = T_{eff}/(2\pi)^3$ at their source. The k-space energy density of blackbody emission from the same region is $T_e/(2\pi)^3$, so that the ratio of fluxes observed is (T_{eff}/T_e). Integrating over frequency (the θ dependence of α is neglected, as for the x mode):

$$\frac{F^{o,NL}}{F_{BB}} = \left(\frac{T_i}{T_e}\right)\left(\frac{\omega_{pe}}{\delta\omega}\right)\left(\frac{2}{3^{3/2}}\right)\left(\frac{a}{\ell}\right)\left(\frac{E}{E_R}\right)\left(\frac{1-q}{q}\right)\left[1 - \left(\frac{p}{1-q}\right)^2\right]$$

$$\times \frac{\left\langle \left(\frac{F^x}{F_{BB}}\right)\left(\frac{\omega}{\omega_{pe}}\right)^2\left(\frac{1}{\delta\omega}\right)\right\rangle}{[u_c\gamma_c - u_R\gamma_R]\ \left[1 + \frac{\delta\omega}{\omega_{pe}}\right]} . \qquad (42)$$

For the parameters of figures 2 and 3, this is $(F^{o,NL}/F_{BB}) \simeq (0.15/\ell)$. If ℓ is smaller than the radius of the spectrometer entrance, this result must be corrected by the fraction of the detector entrance area filled. For Alcator, this is about $(0.3)\ell^4$, so that $(F^{o,NL}/F_{BB}) \simeq 5 \times 10^{-2}$. For $\ell > 2.5$ cm., the detector area is filled, but then $(F^{o,NL}/F_{BB}) \lesssim 6 \times 10^{-2}$, which is thus the upper limit. The fact that the source is cylindrical rather than slablike, will reduce this result further by a factor of approximately (30°/90°) or (1/3).

Reflected o mode emission can also be computed, starting from equation (32). The result is:

$$\frac{F^{o,NL}}{F_{BB}} = 2\sqrt{3}\ \frac{\left(\frac{T_i}{T_e}\right)\left(\frac{\omega_{pe}}{\delta\omega}\right)\left(\frac{v_e}{c}\right)^2\left(\frac{E}{E_R}\right)}{\left(1 + \frac{\delta\omega}{\omega_{pe}}\right)}\ \frac{\left\langle\left(\frac{F^x}{F_{BB}}\right)\left(\frac{\omega}{\omega_{pe}}\right)^2\left(\frac{1}{\delta_\omega}\right)\right\rangle}{[u_c\gamma_c - u_R\gamma_R]}$$

$$\times \left(1 - \alpha_{max}^{-2}\right)\left(\frac{\psi}{(1-\psi^2)^{1/2}}\right) , \qquad (43)$$

which is about 10^{-2} in the case of figures 2 and 3. The net o mode nonlinear emission is then at most about three percent of the blackbody level.

IV. COMPARISON TO OBSERVATIONS

Alcator data are taken for comparison, since they provide clear spectral resolution and polarization measurements. They are, furthermore, similar to spectra seen in other Tokamaks.

Figure 2 shows a fit of the Cerenkov spectral shape to the x mode data where $\eta = 2$. The Cerenkov source has been folded with the detector response to obtain this figure. The response at ω_2 to emission at ω_1 is proportional to $\sin^2[\pi(\omega_2-\omega_1)/\delta\omega]/[\pi(\omega_2-\omega_1)/\delta\omega]^2$. The emission source has also been cut off at the cyclotron frequency at the plasma edge, Ω_E, since most x mode radiation between Ω_E and Ω_o will be absorbed in an intervening upper hybrid layer. The choice of $u_R = 0.8$ satisfies the weak escape condition. The cutoff velocity u_c is chosen as 0.97 to give a reasonable spectral fit. This 1.5 MeV cutoff has smaller discrepancies at both ends of the spectrum than lower or higher cutoffs would have at one end or the other. When u_c is lower, the spectrum slopes upward, and has a greater dip in the center. When u_c is higher, the spectrum flattens out, destroying the dip, and increasing the excess at the upper end. There is, though, also a small increase in emission near the central plasma frequency, which, for cutoffs around three or four MeV., improves the fit at the lower end of the spectrum, so that u_c could be taken somewhat higher. Using these values of u_R and u_c, and the other parameters given in figure 4, formula (17) gives $I_R \simeq$ 2.6 kAmp. The observed ohmic current is 110 kAmp. so that the runaways carry about 2.5 percent of the total current.

For the o mode, a fit to which is shown in figure 3, the same spectral shape is reduced by (p/1-q). While this is 0.5 for the values p = 0.15 and q = 0.7 given by Hutchinson and Komm[4], a value of 2/3 gives a much better fit; this results from a less than ten percent change in each of p and q, well within the limits of uncertainty of those parameters. For the o mode, there is also emission above Ω_E, since x mode emission propagating inward can be reflected and converted to o polarization. This is a fraction (1/2)(p/1-q) of the x mode source, since half of the emission is absorbed in the upper hybrid layer. The source has an inherent cutoff at about 0.9 Ω_o.

In both the x and o mode fits there is a deficiency of emission just above the central plasma frequency. This possibly indicates the need for additional emission, such as the nonlinear process would provide if the acoustic fluctuations were at least two orders of magnitude greater than the thermal level (or if the plasma fluctuations were correspondingly enhanced above their superthermal level). Furthermore, the deficiency is two to three times greater for the o mode, which in general has a more pronounced two peak structure. This is consistent with the ratio of integrated nonlinear o and x emissions estimated from (37), (42), and (43).

Another observed spectrum, this one for the o mode, and for $\eta \simeq 3.2$, is compared to the Cerenkov emission in figure 4. Here $u_R = 0.8$, and $u_c = 0.88$. Lower or higher u_c would produce too little or too much relative emission in the lower part of the spectrum. The fit seems about as good as possible for the present model, in view of the single particle

spectral shapes shown in figure 5. The hollow shape of the resulting spectrum in figure 4 cannot be eliminated by the choice of $f_T(u)$, or by folding in the detector response. Furthermore, the inherent cutoff in the emission at about $0.9\Omega_o$ seems to preclude improving the fit by including emission from particles in a region of lower local plasma frequency. Such particles would contribute more emission in the region (between 1.4 and 2.3 ω_{po} in figure 4) where there is a deficiency of Cerenkov emission from the center of the discharge; however, they would also add that much more to the emission at the upper end of the spectrum, so that the fit of the spectral shape would not be improved.

Since the fit in figure 4 is not good, and requires a cutoff velocity which is too low to justify use of equation (12), it does not give a direct measure of the runaway current, as from equation (17). It is, however, at least true that the Cerenkov emission and the observed spectrum both emit the most at the upper end of the spectrum when $(\Omega/\omega_p)_o$ is increased to 3.2.

V. DISCUSSION

Discrepancies in the fits near ω_{po} suggest the need for significant nonlinear emission at that frequency. Further evidence for such emission is the observation of very narrow, high intensity, sporadic "bursts" of radiation just above ω_{po}. These were first seen several years ago in the "Uragan" stellerator,[18] and more recently in Alcator A and C. In the "Uragan" observations, the detailed spectral structure was resolved, showing emission at $\omega_{pe} + n\omega_{pi}$, for $n \leq 5$. This was interpreted as due to scattering between enhanced plasma oscillations and low frequency fluctuations, generated by linear mode conversion of a superthermal level of sound fluctuations. In Alcator, similar (though unresolved) bursts appear to occur predominantly near the beginning of shots. This may correspond to a stage in the discharge when (T_i/T_e) is small enough to allow a high level of sound fluctuations. Another possible source of the fluctuations is from drift waves, which are greatly enhanced, as evidenced by their effect on the plasma energy transport. A further constraint on the low frequency fluctuations, and the nonlinear emission process, is that such a process must be suppressed for parameters such as those corresponding to the spectrum in figure 4.

As for the discrepancies in the fit at intermediate values of ω, as in figure 4, relativistically shifted emission from the first cyclotron harmonic may account for some of the deficiency. This would correspond to the fact that at higher values of $(\Omega/\omega_p)_o$, enhanced emission is observed between the first and second cyclotron harmonics, since the relativistically shifted emission is expected to occur both above and below the cyclotron frequency.[5]

Despite these and other remaining problems, the observations, such as those shown in figures 2 and 3, give a direct measure of the runaway current, and allow determination of an approximate runaway cutoff velocity. This demonstrates new diagnostic value for such spectral data.

ACKNOWLEDGMENTS

The numerical computations for this paper were done on MACSYMA, a symbolic computation system at the Laboratory of Computer Science, Massachusetts Institute of Technology.

This research was supported by the United States Department of Energy, contract number DE-AC02-78ET51013.

VI. REFERENCES

1. TFR Group and NPL Submillimeter-Wave Group, in Proceedings of the Seventh European Conference on Controlled Fusion and Plasma Physics, Lausanne, Switzerland, 1975 (European Physical Society, Geneva, 1975).
2. P. Brossier, A. E. Costley, D. S. Komm, G. Ramponi, and S. Tamor, in Proceedings of the Sixth International Conference on Plasma Physics and Controlled Nuclear Fusion Research, Berchtesgaden, West Germany, 1976 (International Atomic Energy Agency, Vienna, 1977), Vol. 1, p. 409.
3. A.E. Costley and TFR Group, Phys. Rev. Lett. 38, 1477 (1977).
4. I.H. Hutchinson and D.S. Komm, Nucl. Fusion 17, 1077 (1977).
5. I.H. Hutchinson, Infrared Physics 18, 763 (1978).
6. H.P. Freund, L.C. Lee, and C.S. Wu, Phys. Rev. Lett. 40, 1563 (1978).
7. H. P. Freund, L.C. Lee, and C.S. Wu, Univ. of Maryland Technical Note BN-886 (1978).
8. K. Swartz, I.H. Hutchinson, and K. Molvig, Bull. Amer. Phys. Soc. 23, 888 (1978).
9. I.H. Hutchinson, K. Molvig, and S.Y. Yuen, Phys. Rev. Lett. 40, 1091 (1978).
10. J. Fidone, G. Ramponi, and P. Brossier, Phys. Fluids 21, 237 (1978).
11. K. Molvig, M.S. Tekula, and A. Bers, Phys. Rev. Lett. 38, 1404 (1977).
12. A.G. Sitenko and A.A. Kolomenskii, Sov. Physics JETP 3, 410 (1956).

13. M. Bornatici and F. Englemann, Phys. Fluids 22, 1409 (1979).

14. I.B. Bernstein, Phys. Fluids 18, 320 (1975).

15. G. Bekefi, Radiation Processes in Plasmas (Wiley, New York, 1966), p. 236.

16. R.C. Davidson, Methods in Nonlinear Plasma Theory (Academic Press, New York, 1972), Chapter 13.

17. N. Krall and A. Trivelpiece, Principles of Plasma Physics (McGraw-Hill, New York, 1973) p. 568.

18. A.V. Longinov, N.F. Perepelkin, and V.A. Suprunenko, Sov. J. Plasma Physics 2, 344 (1976).

FIGURE CAPTIONS

Fig. 1 Contour plot of $u(\omega/\omega_{po}, \cos\theta)$ in $(\omega/\omega_{po}, \theta)$ plane. $(\Omega/\omega_p)_o = 3$.

Fig. 2 Observed x emission in Alcator (figure 7 of reference 5) for average electron density $\bar{n}_e \simeq 6 \times 10^{13}$ cm.$^{-3}$, $B_o \simeq 61$ kG., toroidal electric field $E \simeq 1$ V./m., and $T_{eo} \simeq 1$ keV., compared to Cerenkov emission for $(\Omega/\omega_p)_o = 2$. The blackbody level is normalized to the second cyclotron harmonic, not shown. In Eqs. (13) and (17) $\omega_1 = 1.1\omega_{po}$, $\Delta\omega = 0.2\ \omega_{po}$, $\left\langle F^x/F_{BB} \right\rangle = 5.0$, and $\left\langle (\omega/\omega_{po})^2 \right\rangle = 1.4$.

Fig. 3 Same is figure 2, but for o mode.

Fig. 4 Observed o emission in Alcator (figure 8(c) of reference 5) for $\bar{n}_e \simeq 4 \times 10^{13}$cm.$^{-3}$, $B_o \simeq 79$kG, and $T_{eo} \simeq 1$ keV., compared to Cerenkov emission for $(\Omega/\omega_p)_o = 3.16$. The blackbody level is determined as in figure 2.

Fig. 5 Single particle emission spectra, normalized to the same height, for particles of different velocities, when $(\Omega/\omega_p)_o = 3.16$.

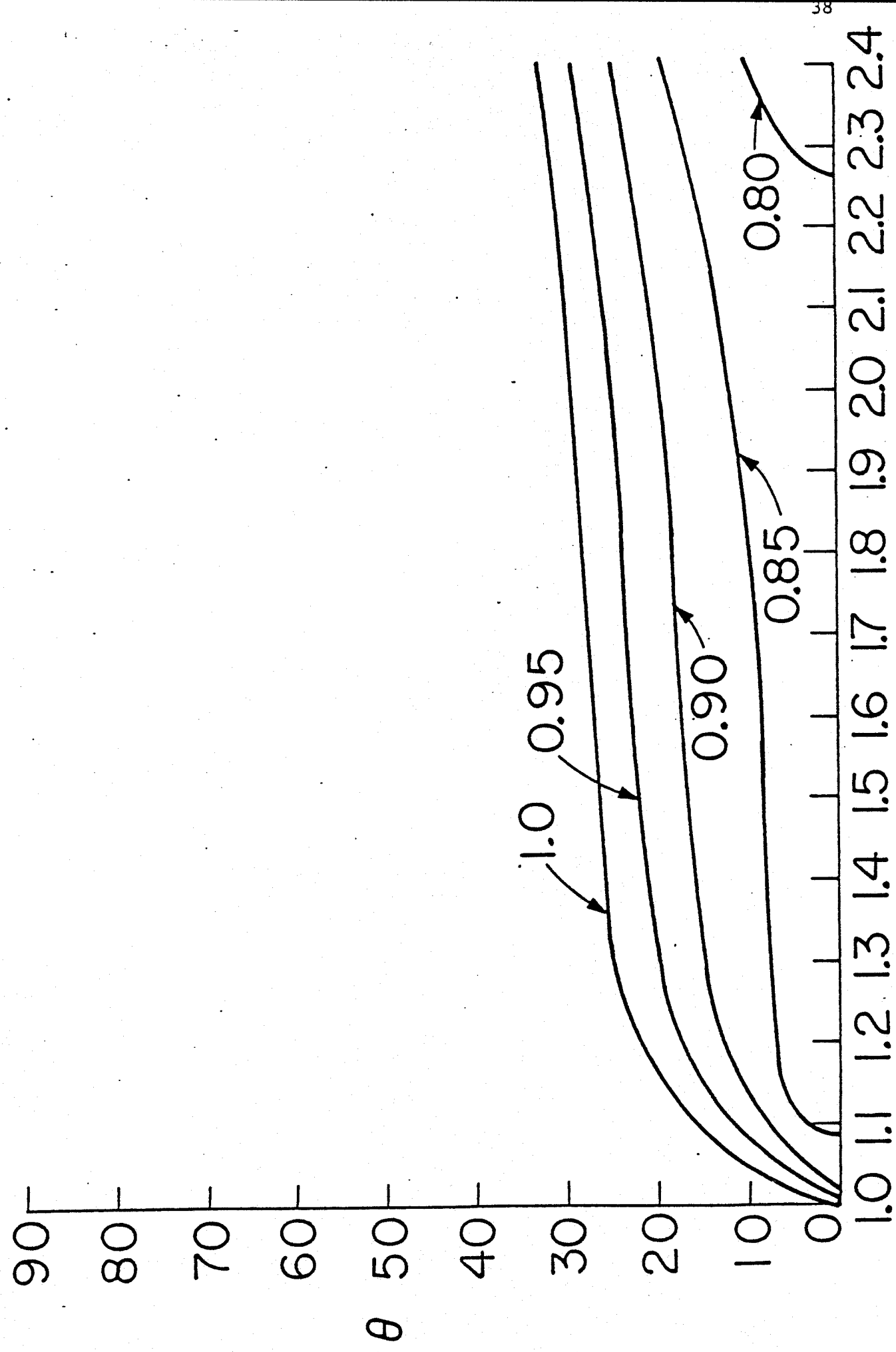
θ
0
10
20
30
40
50
60
70
80
90
1.0
1.1
1.2
1.3
1.4
1.5
1.6
1.7
1.8
1.9
2.0
2.1
2.2
2.3
2.4
ω/ωpo
1.0
0.95
0.90
0.85
0.80

Fig. 1

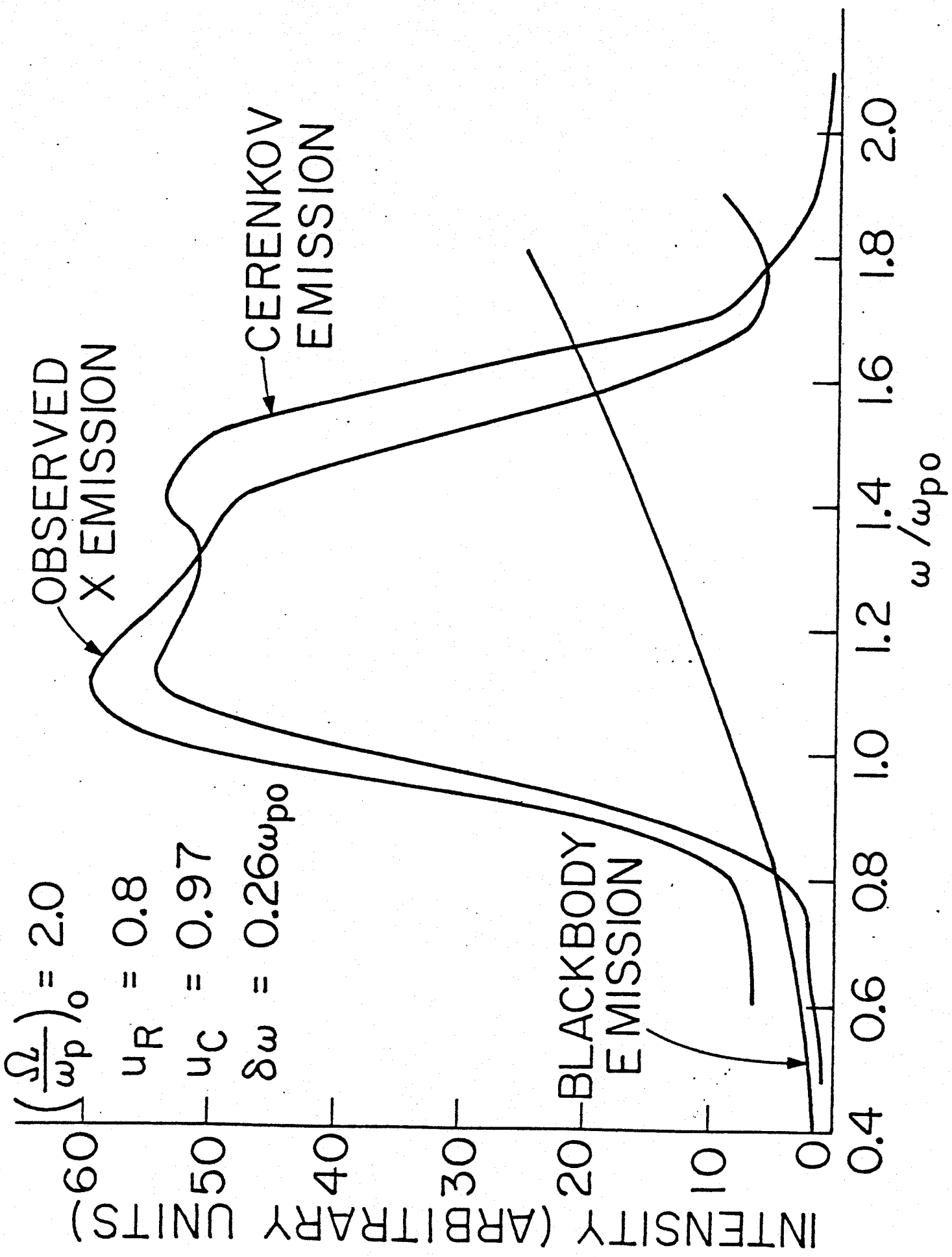
OBSERVED
X EMISSION
CERENKOV
EMISSION
BLACKBODY
EMISSION
$(\frac{\Omega}{\omega_p})_o = 2.0$
$u_R = 0.8$
$u_C = 0.97$
$\delta\omega = 0.26\omega_{po}$
INTENSITY (ARBITRARY UNITS)
0
10
20
30
40
50
60
0.4
0.6
0.8
1.0
1.2
1.4
1.6
1.8
2.0
ω/ω_{po}

Fig. 2

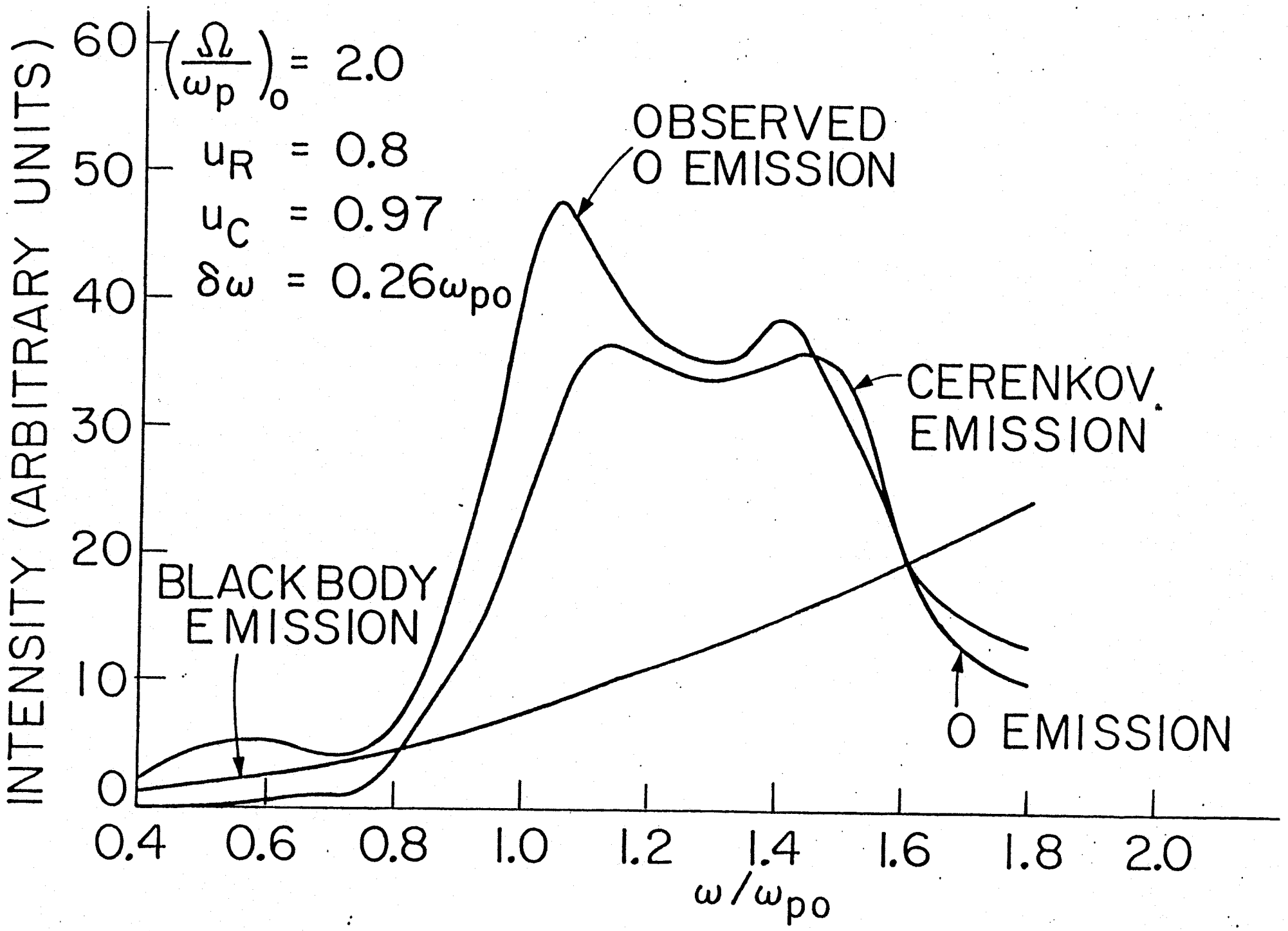
INTENSITY (ARBITRARY UNITS)
60
50
40
30
20
10
0
$\left(\frac{\Omega}{\omega_p}\right)_o = 2.0$
$u_R = 0.8$
$u_C = 0.97$
$\delta\omega = 0.26\omega_{po}$
OBSERVED
O EMISSION
CERENKOV
EMISSION
BLACK BODY
EMISSION
O EMISSION
0.4
0.6
0.8
1.0
1.2
1.4
1.6
1.8
2.0
ω/ω_{po}

Fig. 3

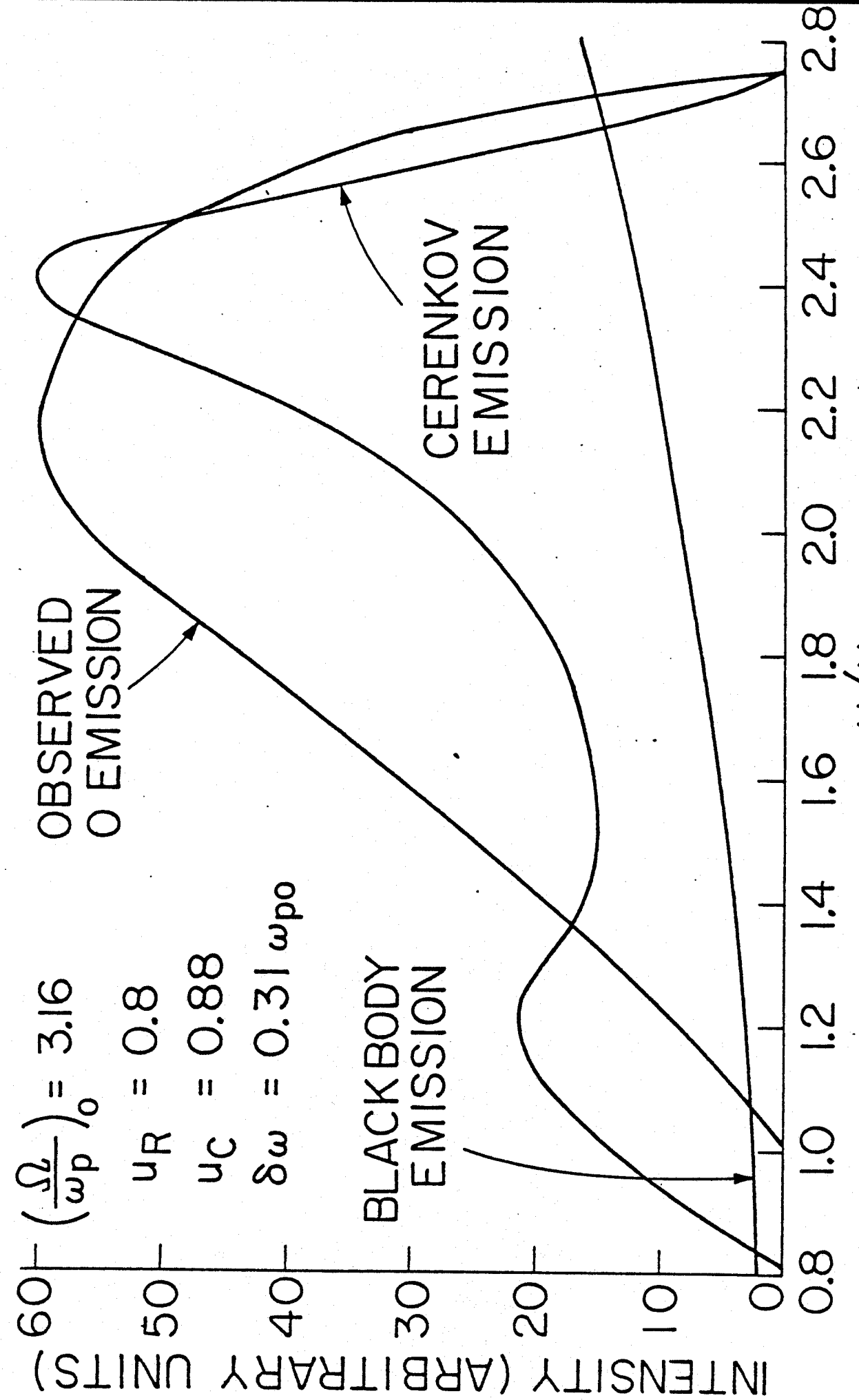
INTENSITY (ARBITRARY UNITS)
60
50
40
30
20
10
0
0.8
1.0
1.2
1.4
1.6
1.8
2.0
2.2
2.4
2.6
2.8
ω/ωpo
OBSERVED
O EMISSION
CERENKOV
EMISSION
BLACKBODY
EMISSION
(Ω/ωp)o = 3.16
uR = 0.8
uC = 0.88
δω = 0.31 ωpo

Fig. 4

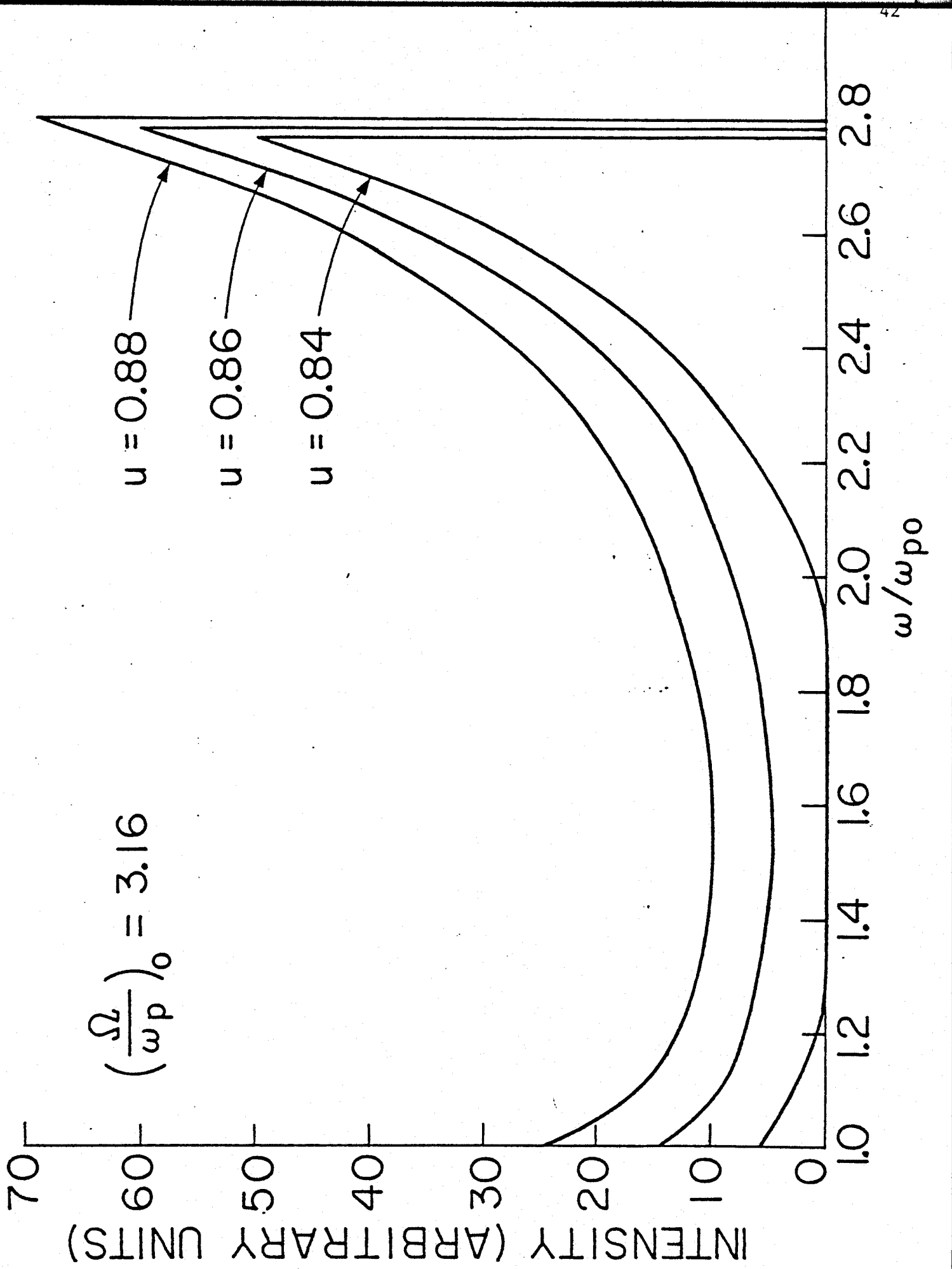
INTENSITY (ARBITRARY UNITS)
0
10
20
30
40
50
60
70
1.0
1.2
1.4
1.6
1.8
2.0
2.2
2.4
2.6
2.8
ω/ωpo
u = 0.88
u = 0.86
u = 0.84
(Ω/ωp)o = 3.16

Fig. 5